

A&A manuscript no.
(will be inserted by hand later)

Your thesaurus codes are:
11.03.1; 11.03.4; 11.04.1; 11.11.1; 12.03.3

ASTRONOMY
AND
ASTROPHYSICS

Abell 521: Dynamical analysis of a young cluster ^{*}

S.Maurogordato¹, D.Proust², T.C. Beers³, M. Arnaud⁴, R. Pelló⁵, A.Cappi⁶, E.Slezak¹, J.R. Kriessler⁷

¹ Observatoire de Nice, B4229, Le Mont-Gros, 06304 Nice Cedex 4, E-Mail: maurogor@obs-nice.fr

² DAEC, CNRS, Observatoire de Paris-Meudon, 5 place J. Janssen, 92195 Meudon, France, E-Mail: proust@obspm.fr

³ Department of Physics & Astronomy, Michigan State University,
E. Lansing, MI 48824, USA, Email: beers@pa.msu.edu

⁴ CEA/DSM/DAPNIA/Service d'Astrophysique, CEA/Saclay, F-91191 Gif sur Yvette Cedex, France E-Mail arnaud@hep.saclay.cea.fr

⁵ Observatoire Midi-Pyrénées, Avenue E.Belin, Toulouse E-Mail: roser@astro.obs-mip.fr

⁶ Osservatorio Astronomico di Bologna, via Zamboni 33, I-40126 Bologna, Italy, E-Mail: cappi@astbo3.bo.astro.it

⁷ Department of Astronomy, University of Minnesota, 116 Church St. S.E., Minneapolis, MN 55455, USA, Email: jeffk@isis.spa.umn.edu

Submitted 1999 January 21

Abstract. We present the results of a dynamical analysis of the rich X-Ray luminous galaxy cluster Abell 521, and discuss the nature of the arc-like structure first noted by Maurogordato et al. (1996). Our study is based on radial velocities for 41 cluster members, measured from spectra obtained at the European Southern Observatory and the Canada-France-Hawaii Telescope. Based on statistical analyses performed with the ROSTAT package, we find that Abell 521 is an intermediate-redshift cluster ($C_{BI} = 74132^{+202}_{-250}$ km/s) with a rather high apparent value of the velocity dispersion $S_{BI} = 1386^{+206}_{-139}$ km/s.

There are many indications that this cluster is presently undergoing strong dynamical evolution: a) the high value of the velocity dispersion, which cannot be explained by trivial projection effects, b) significant clumping in the two-dimensional projected positions of the galaxies in the cluster, quantified by a mixture-model three-group partition significant at 99 % level, c) the extreme value of the velocity dispersion ($\sigma \sim 2000$ km/s) in a central high density NE/SW structure, d) a strong increase of the velocity dispersion as determined from the reddest and bluest galaxies, suggesting that cluster spirals are not yet virialized; e) the presence of multiple nuclei in the core of the brightest cluster galaxy, one of which has a statistically significant velocity offset from the rest of the cluster members, and f) an apparently different stellar population for the various knots of the arc candidate which changes along the structure.

The two brightest knots of the giant arc candidate are shown to be at the velocity of the cluster. This makes the

gravitational lensing interpretation for the bright curved structure very improbable, although gravitational lensing might still be present in this cluster, as suggested by the colors of two fainter arclet-like structures.

Key words: Galaxies: clusters: general – Galaxies: clusters: individual (Abell 521) – Galaxies: distances and redshifts – Galaxies: kinematics and dynamics – Cosmology: observations

1. Introduction

Clusters of galaxies are complex, evolving systems which present numerous observational and theoretical challenges, yet the scientific payoff of a detailed understanding of these structures is also great. The determination of the total gravitationally-bound mass, the relative distribution of visible (galaxies and hot gas) and dark matter, and the dynamics of galaxies in clusters all provide essential information for testing models of galaxy formation and evolution.

There exist numerous uncertainties in deriving the mass distribution within clusters from optical observations alone (Merritt and Gebhardt 1995). X-ray observations of the hot gas in clusters permit significant progress in our understanding of cluster dark matter distributions. The two approaches are complementary, but in both instance strong assumptions are required for recovering the mass distribution. In particular, the optical approach (through the virial analysis) requires one to adopt hypotheses concerning the orbital distribution of member galaxies, while the X-ray approach assumes that the hot gas is in hydrostatic equilibrium within (presumably) a single cluster potential well. A comparison of both methods, when possible, gives the opportunity to test the underlying hy-

Send offprint requests to: Sophie Maurogordato

^{*} Based on observations made at the Canada France Hawaii Telescope (CFHT) and at the European Southern Observatory. CFHT is operated by the National Research Council of Canada, the Centre National de la Recherche Scientifique of France, and the University of Hawaii.

potheses and to better constrain the model parameters (Henry et al. 1993). With this aim in mind, we have initiated a combined X-ray and optical observational program, including both imaging and multi-object spectroscopy at ESO and the CFHT, on a selected sample of clusters at intermediate redshifts. Our sample was defined in order to cover a variety of clusters, which could be taken as representative of a range of dynamical states.

Abell 521 is a distant (Abell distance class 6), relatively rich (Abell richness class 1), southern cluster, morphologically classified as Bautz-Morgan Type III (Abell 1958; Abell, Corwin, and Olowin 1989). This cluster was shown by the HEAO-1 survey to be a bright X-ray source (Kowalski et al. 1984). In images taken to select spectroscopic targets in the fields of this cluster, we detected several arc candidates (Maurogordato et al. 1996). This was not surprising, as it is suggested by theoretical studies of the gravitational lensing phenomenon that luminous arcs should be frequently found in the centers of distant X-ray luminous clusters (Le Fèvre et al. 1995). In our case, the detection of luminous arcs, *if real*, is important because they provide an independent means to measure the *total* mass of the cluster, without requiring explicit models of the mass distribution (Fort and Mellier 1994). All this motivated us to focus on this cluster for deeper analysis, mainly through multi-object spectroscopy, to probe its dynamical state, long-slit spectroscopy to test the reality of the arc and arclet candidates, and multi-band photometry of the central region, with X-Ray imaging and spectroscopy being conducted in parallel. A comparison of the X-Ray, optical images and temperature measurement of the main cluster will be presented in Arnaud et al. (1999); a photometric redshift analysis of the arc candidates from multicolor photometry will appear in Pelló et al. (1999).

Section 2 of this paper presents the spectroscopic data we have obtained to date in our observational campaign on this cluster. Section 3 is an analysis of the velocity distribution. In section 4 we discuss the nature of the brightest cluster galaxy, and the reality of the gravitational arc candidates which have been suggested previously. In the following, unless explicitly specified, we have used $H_0 = 50h_{50}\text{kms}^{-1}\text{Mpc}^{-1}$, and $q_0 = 0.5$.

2. Observations and data reduction

Multi-object spectroscopic observations of Abell 521 were carried out at the ESO 3.6m telescope in December 1995 and at the CFHT in March 1997. At ESO, we used the Faint Object Spectrograph and Camera with the grism O300, yielding a dispersion of $230\text{\AA}/\text{mm}$, and the TEK512 CCD chip ($27\mu\text{m}$ 512×512 pixels); at CFHT we used the Multi Object Spectrograph facilities (Le Fèvre et al. 1994) with the grating O300, resulting in a dispersion of $240\text{\AA}/\text{mm}$, and the STIS2 CCD ($21\mu\text{m}$ 2048×2048 pixels). These combinations of gratings and detectors result in dispersions of $6.3\text{\AA}/\text{pixel}$ and $5\text{\AA}/\text{pixel}$, respectively.

Typically, two exposures, of 2700s each, were taken for fields across the cluster. Wavelength calibration was done using arc lamps before each exposure (Helium-Argon, and Helium-Neon lamps). Data reduction was carried out with IRAF¹, using the MULTIREDD package (Le Fèvre et al. 1995). Radial velocities were determined using the cross-correlation technique (Tonry and Davis 1981) implemented in the RVSAO package (developed at the Smithsonian Astrophysical Observatory) with radial velocities standards obtained from observations of late-type stars and previously well-studied galaxies.

We have obtained 65 spectra of objects in the region of Abell 521. Star contamination was very low (only 3 of the 65 targets turned out to be stars). From these data we have retained 49 spectra of galaxies with a signal-to-noise ratio sufficiently high to derive the measurement of the radial velocity with good confidence (with the parameter R parameter of Tonry and Davis greater than 3). This results in a completeness of our velocity sample of 30% of the galaxies brighter than $m_V = 21$. The finding chart for the objects with measured velocities is shown in Figure 1. Spectra of the brightest BCG components were obtained with EFOSC at ESO using the long-slit mode, and 3 different exposures (2×2700 sec and 1800 sec). Imaging of Abell 521 was obtained in 1994 at the CFHT with the MOS in B and R (using the LORAL3 CCD) and in 1997 in the V and I bands (using the STIS2 CCD); the definition and analysis of the galaxy catalog from the V-band image are presented in Arnaud et al. 1999 and the complete photometric catalog will be provided in Slezak et al. 1999. Also a J image of the cluster core was obtained in November 1996 at the CFHT with OSIS and 1800 sec of equivalent exposure (see Pelló et al. 1999). Velocity measurements from our spectroscopy are listed in Table 1. The columns are as follows: column (1): Identification number of each target galaxy in the cluster as shown in the finding charts; Columns (2) and (3): Right ascension and Declination (J2000.0) of the target galaxy; Column (4): Best estimate of the radial velocity resulting from the cross-correlation technique; Column (5): estimated error; Column (6): a listing of detected emission lines. Galaxies 1-21 were observed at CFHT, while those from 22-49 were obtained at ESO.

3. Velocity distribution in Abell 521

3.1. Global mean velocity and velocity dispersion of the cluster

From a visual inspection of the cone diagram displayed in Figure 2, we selected a reasonable range of velocities (70000 to 80000 km/s) as candidate members of the clus-

¹ IRAF is distributed by the National Optical Astronomy Observatories, which are operated by the Association of Universities for Research in Astronomy, Inc., under cooperative agreement with the National Science Foundation

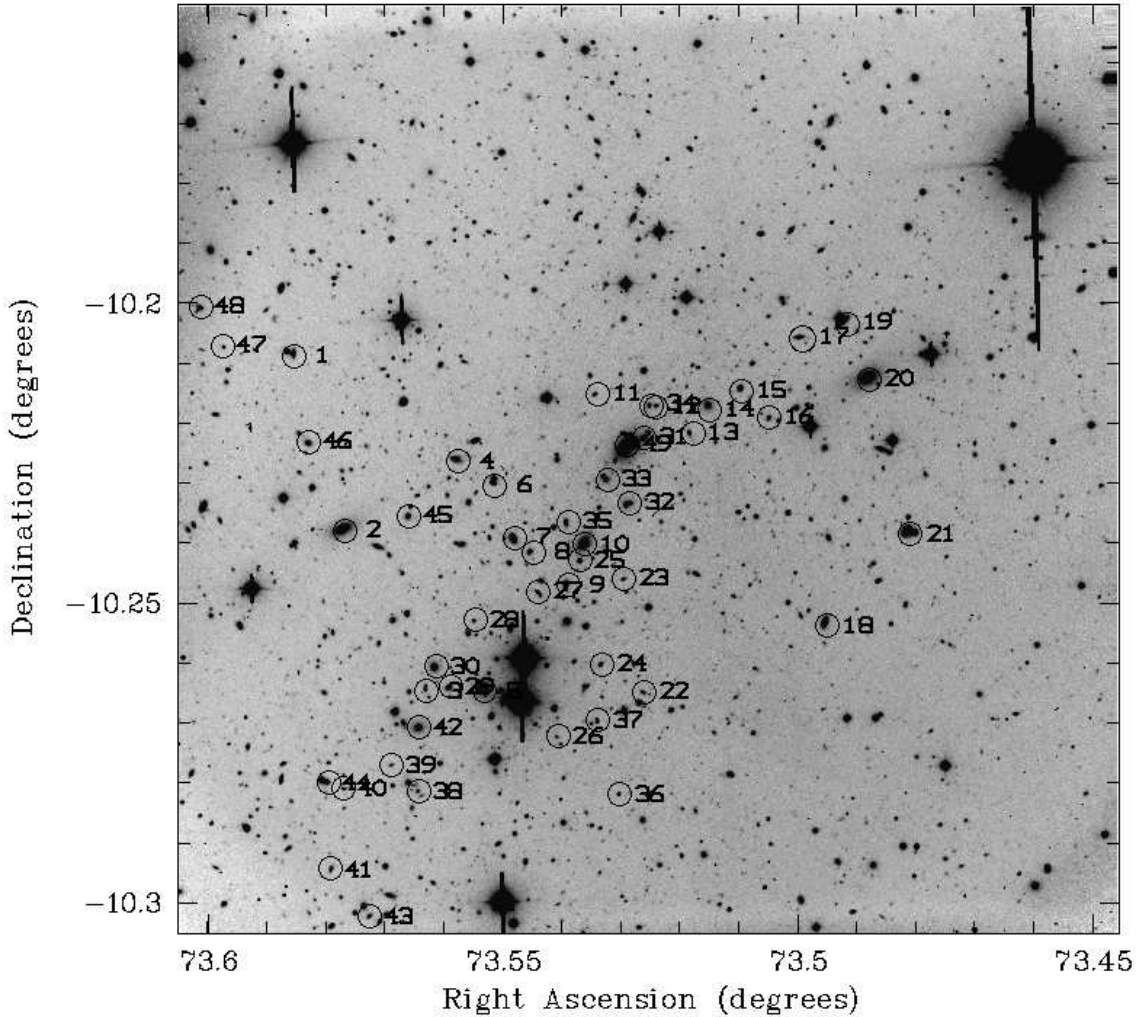


Fig. 1. Finding chart for galaxies with successful velocity measurements in Abell 521. The galaxies are labeled as in Table 1.

ter. One galaxy (number 2) is identified as a clear foreground object. Three background objects are found at a redshift $z \sim 0.295$; others are at redshifts of 0.289, 0.31 and 0.331.

We have employed the ROSTAT package (Beers, Flynn, and Gebhardt 1990, hereafter BFG) to analyze the velocity distribution of the 41 remaining galaxies in the selected velocity range. In order to quantify the central location and scale of the velocity distribution for Abell 521, we have used the resistant and robust biweight estimators (C_{BI} and S_{BI} , respectively) recommended by BFG. For the complete sample of velocities, we obtain $C_{BI} = 74132^{+202}_{-250}$ km/s and $S_{BI} = 1386^{+206}_{-139}$ km/s. Values obtained with other estimators show similar values. The one-sigma errors in these quantities are calculated in ROSTAT by bootstrap re-sampling of 1000 subsamples of the velocity data.

In Figure 3 (top) we show a stripe density plot of the velocity distribution for Abell 521. The velocity his-

togram, calculated with a binning of 1000 km/s, is shown in Figure 3 (bottom), along with a superposed Gaussian of standard deviation 1386 km/s, shifted to the velocity of the cluster. The radial velocity of the brightest cluster galaxy (hereafter) BCG is shown with an arrow.

The apparent velocity dispersion of Abell 521, $\sigma \sim 1400$ km/s, is among the largest values observed in galaxy clusters, as compared, for example to the velocity dispersion distribution of the recent ENACS survey (Mazure et al. 1996), and it is well above the median value of 744 km/s estimated by Zabludoff et al. (1990) for a sample of 65 clusters. However, the velocity dispersion of Abell 521 is significantly *larger* than the value ($\sigma = 1017 \pm 65$ km/s) we would predict from X-ray observations, using our measurement of the gas temperature, and assuming equipartition between kinetical and potential energy (Arnaud et al. 1999).

We endeavor to determine how reliable this estimate of the velocity dispersion is, and whether or not it is affected

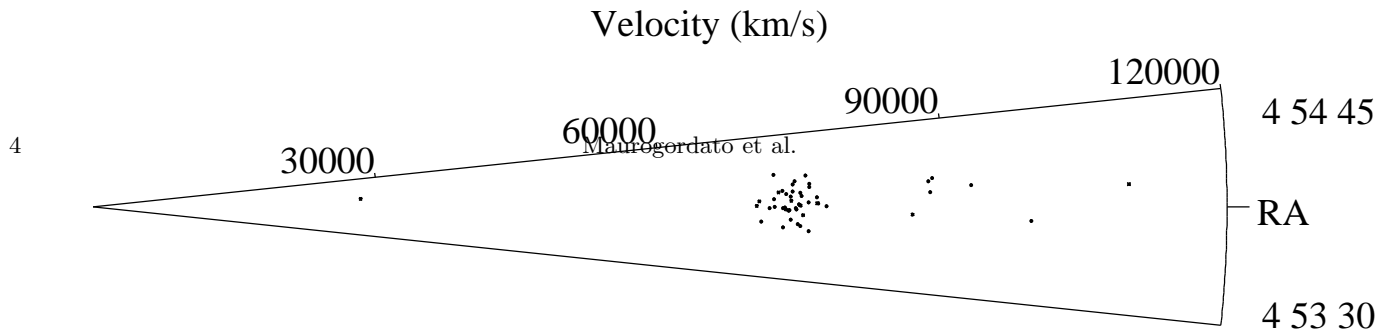


Fig. 2. Distribution in Right Ascension versus radial velocity for 49 galaxies in the inner $10' \times 10'$ region of Abell 521.

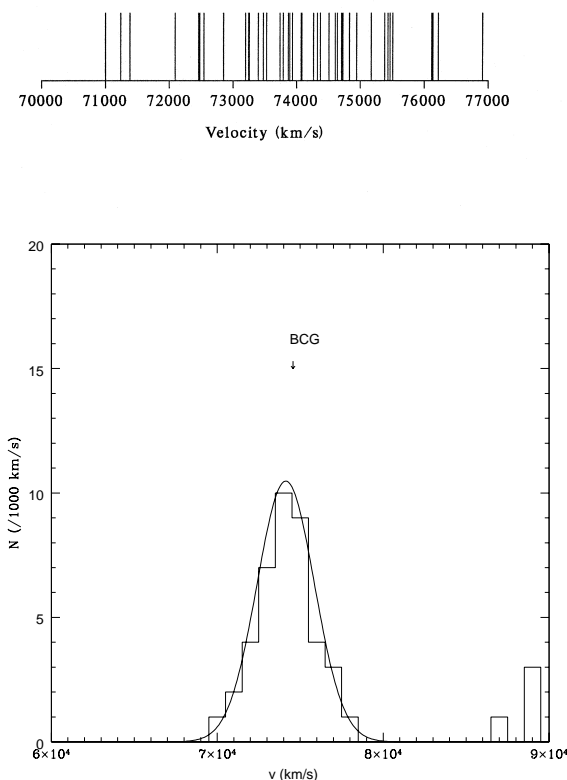


Fig. 3. (Top) Stripe density plot of radial velocities for presumed members of Abell 521. The velocity of the BCG is shown with an arrow. (Bottom) The radial velocity histogram, calculated with a binning of 1000 km/s, in a $10' \times 10'$ region centered on Abell 521. A Gaussian of standard deviation 1386km/s, shifted to the velocity of the cluster, is superimposed.

by various problems such as subclustering or contamination by outliers. A fair assessment of the impact of potential interlopers is essential for derivation of an unbiased measurement of the velocity dispersion (see for instance

Mazure et al. 1996). Given that the spatial coverage of our velocity sample is far from complete, and strongly favors the high-density regions, and the limitations imposed by the relatively small number of measured velocities, we cannot proceed to a sophisticated analysis of subclustering. For the present, we limit ourselves to classical tests which examine whether our velocity measurements are drawn from a single parent population, or are drawn from a mix of slightly-offset velocity distributions which, taken as a single kinematic entity, would mimic this large velocity dispersion.

3.2. Simple statistical tests of the velocity distribution

We have performed a number of statistical tests of the velocity data for Abell 521. All twelve of tests implemented in ROSTAT are consistent with the hypothesis that the velocities are drawn from a Gaussian parent population. We also searched for the existence of statistically significant gaps in the velocity distribution, which can indicate the possible presence of subclustering, especially when located in the center of a distribution – none were found. Bird and Beers (1993) discuss alternative measures of the classical coefficients of skewness and kurtosis, the asymmetry (AI) and tail indices (TI), which are useful for detecting subtle deviations from normality in distributions. For the complete velocity set, we obtain $AI = -0.238$ and $TI = 1.165$, respectively. Neither of these values allow rejection of a Gaussian parent population according to the tables supplied by Bird and Beers.

While we cannot exclude some contamination from outliers or groups along the line-of-sight to Abell 521, these results do exclude the presence of significant projection effects in velocity space.

3.3. Testing for substructure in the projected and redshift distribution

To search for the presence of substructure in the projected galaxy distribution of Abell 521 we have fit the observed galaxy positions to a number of Gaussian mixture models, following the procedures described in Kriessler and Beers

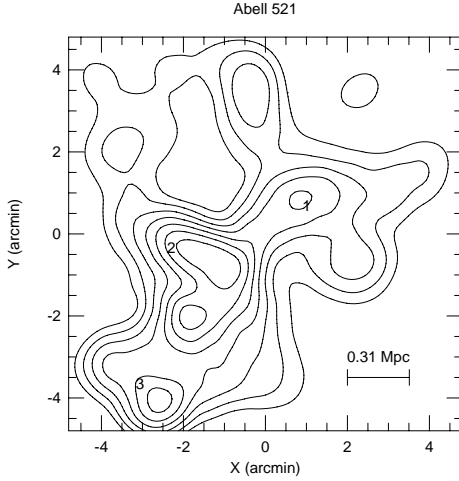


Fig. 4. Adaptive kernel contour map of the projected galaxy distribution for galaxies brighter than $m_V = 22.0$. The centers of the three subclusters corresponding to the KMM best partition are numbered as in Table 2. The minimum contour corresponds to a level of 3.638 galaxies/arcmin²; the contours are linearly spaced with a separation of 1.073 galaxies/arcmin².

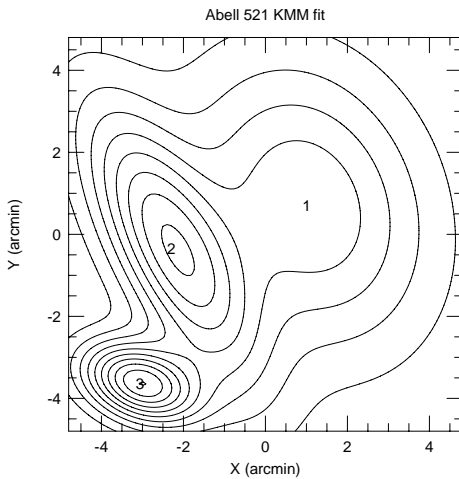


Fig. 5. Reconstructed contour maps of the three best-fit two-dimensional Gaussians obtained from the KMM analysis (Table 2). The minimum contour corresponds to a level of 0.130 galaxies/arcmin²; the contours are linearly spaced with a separation of 1.329 galaxies/arcmin².

(1997). In this analysis we have only used the ~ 400 galaxies brighter than $m_V = 22.0$, to limit contamination from background galaxies projected on the face of the cluster. Figure 4 shows an adaptive-kernel contour map of the region centered on Abell 521.

The best-fit KMM partition of the projected galaxy positions, evaluated using a maximum-likelihood ratio test and a bootstrap procedure, is a three-group partition which is significant at the 99% level (parameters of the partition are specified in Table 2). Column (1) of this table lists the identification number of the group (indicated in Figure 4). Column (2) lists the number of galaxies assigned to each group. Columns (3) and (4) list the fraction of the total number of galaxies present in each group, and the fraction of total luminosity in each group, respectively. The x and y positions of the groups, along with their one-sigma errors, are listed in columns (5) and (6). The median magnitude of the galaxies within each group is listed in column (7); column (8) lists the mean magnitude of the 10th to 20th brightest galaxies in each group.

From the application of a K-S test to the magnitude distributions of the various groups, we find that group 3 is marginally fainter than the others. This, along with the fainter value of m_{10-20} (see Jones and Mazure 1996), suggests that group 3 may contain a large fraction of background galaxies. Figure 5 shows the reconstructed contour maps of the three Gaussians corresponding to the best-fit partition obtained with the KMM algorithm.

We next obtain a split of the velocity sample, assigning each galaxy to a group associated to the nearest projected group center obtained from the KMM analysis. This results in 9 galaxies associated with KMM1, 19 with KMM2, and 2 galaxies with KMM3. Galaxies located farther than 1.5 arcmin from any of the group centers are set aside.

We then obtain a further split of the KMM2 group into two components: KMM2 North (14 galaxies) and KMM2 South (5 galaxies) in order to isolate the Southern extension of KMM2 seen in the adaptive kernel map shown in Figure 4. There are only two galaxies with measured velocities assigned to the KMM3 region (numbers 40 and 42), both of which have slightly higher velocities than the adopted central location velocity for the cluster as a whole. More measured velocities are required to reliably determine the mean velocity of KMM3.

We are thus left with three subsamples of the velocity catalog on which we have run the ROSTAT package, corresponding to regions KMM1, KMM2 North, and KMM2 South. The results of this analysis are summarized in Table 3. Although the small number of velocities in each subsample do not allow us to derive precise measurements of the velocity dispersion, two qualitative conclusions can be drawn. First, there are no significant velocity offsets between the individual partitions with respect to one another, at least to within the bootstrapped errors on the velocity locations. Second, the KMM2 North partition has a significantly higher value of the velocity dispersion than the other two partitions, or as compared to the cluster as a whole. This result is also strikingly clear on the stripe density plots of these three partitions displayed in Figure 6. The KMM2 North group, which includes the so-called “ridge” structure described by Arnaud et al. (1999), is

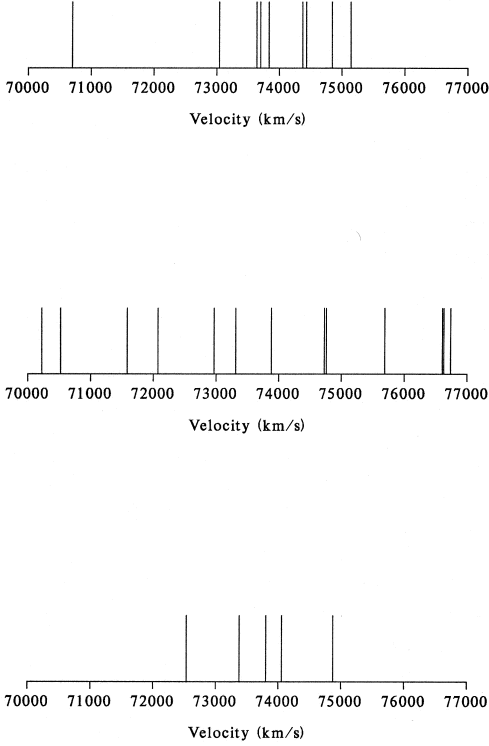


Fig. 6. Stripe density plots of radial velocities for the three partitions analysed with ROSTAT – from top to bottom: KMM1 , KMM2 North, and KMM2 South.

probably kinematically complex, and may well be comprised of several subclusters.

We have also examined the location of the three galaxies with $z \sim 0.295$ (objects 4, 40, and 46) to check if they are spatially clustered, as would be expected for a background group. These galaxies are all located in the Eastern part of the cluster. Taking into account the velocity measurement in Table 1, galaxies 4 and 46 are separated from one another by $\sim 3.2h_{50}^{-1}$ Mpc, and lie at the Eastern part of the KMM2 structure. Galaxy 40 lies $\sim 2.4h_{50}^{-1}$ Mpc apart galaxy 4, and $\sim 5.2h_{50}^{-1}$ Mpc apart galaxy 46 in the Southern direction. It is thus not excluded that these three galaxies are members of a background loose group, but a much more complete redshift survey of Abell 521 is required to resolve this question.

3.4. Analysis of the velocity distribution with the color index

Several analyses have shown that the velocity distribution of galaxies in clusters can be very different for individual morphological types (e.g., see the analysis by Binggelli et al. 1987 on the Virgo Cluster, Beers et al. 1992 on A400,

Bird et al. 1995 on Abell 151, and of Girardi et al. 1996 on a larger sample of clusters). A higher value of velocity dispersion is generally found for late-type galaxies, as compared to early types, which is expected if the latter have fallen into the cluster potential following the initial collapse (Tully and Shaya 1984). The spatial resolution of our imaging data for Abell 521 is unfortunately not sufficient to assign a morphological type to all the objects with measured velocities, in particular at the faintest magnitudes. As an alternative, we have used the color indices of the galaxies in order to define two subsamples within our velocity catalog, with values of $B - R$ respectively higher and lower than the median value for the sample as a whole. In the following we refer to these as the “red” and “blue” subsamples.

Inspection of the brightest galaxies, whose morphological type is unequivocally determined by eye, shows that typical cluster ellipticals belong to the *red* subsample, and spirals to the *blue* subsample. Galaxies of the cluster with detected emission lines (Table 1) belong to the *blue* subsample, as expected. Figure 7 shows stripe density plots of the velocity distributions for the *red* and *blue* subsamples. These subsets appear rather different. ROSTAT analysis of the two subsamples yields values of $C_{BI} = 74125_{-273}^{+218}$ km/s and $S_{BI} = 1011_{-108}^{+214}$ km/s for the *red* subsample of 19 galaxies, and $C_{BI} = 73924_{-445}^{+408}$ km/s and $S_{BI} = 1803_{-191}^{+256}$ km/s for the *blue* subsample of 20 galaxies, respectively. The central locations on velocity of the high and low $B - R$ subsamples are consistent with one another, but the velocity scales are significantly different. We have further checked how stable these results are by testing different subsamples obtained by translating the color cut on $B - R$ within 1σ around the median value. The range is of course limited, as the number of objects falls rapidly when moving off the median. The values of the dispersions which are obtained fluctuate $\sim 20\%$ around the previously calculated ones, but the general trend remains true and becomes even more more accentuated when taking only the most extreme regions of the color distribution. In any case, the velocity distribution of the *blue* subsample is quite large, while the *red* subsample shows a value which is typical of other galaxy clusters.

One might wonder if the colors of the galaxies are correlated with the high-density structures evidenced in the V-band density map. Based on our inspection of the color indexes, there might be a color segregation in the various structures, with a bluer NE/SW extension including KMM2 North and more compact redder clumps along the NW/SE extension. However the bluest galaxies belonging to our velocity sample are distributed across the entire field of the cluster, so the high velocity dispersion of these galaxies cannot be due solely to the contribution of the KMM2 North region.

The higher velocity dispersion of the *blue* subsample can be explained under the hypothesis that Abell 521 is

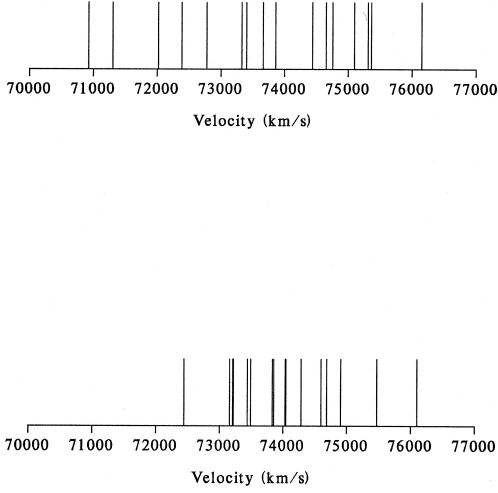


Fig. 7. Stripe density plots of radial velocities for the two subsamples split according to color index: (Top) the *blue* subsample, and (Bottom) the *red* subsample.

in fact dynamically complex, and one might expect this class of galaxies includes many spirals which are not yet virialized within the cluster potential. In this case the distribution of spirals would be much more dispersed than that of ellipticals (Girardi et al. 1996). In fact, the velocity dispersion as estimated from the *red* subsample, $S_{BI} = 1011^{+214}_{-108}$ km/s, is quite in line with the predicted cluster dispersion based on the X-ray analysis, which is at variance with the dispersion based on the entire set of galaxies with measured velocities.

4. The region surrounding the brightest cluster member

4.1. The brightest cluster galaxies in Abell 521

In Figure 8 we show a one arcmin subframe of the 600s R image centered on the BCG in Abell 521. This galaxy has a magnitude $m_V = 17.22$, which corresponds to a K-corrected absolute magnitude $M_V = -24.37 + 5 \log h_{50}$. Two other gE galaxies are present in the core of Abell 521, identified in Figure 1 as objects 10 and 20 with magnitudes 18.71 ($M_V = -22.90 + 5 \log h_{50}$) and 18.67 ($M_V = -22.86 + 5 \log h_{50}$), and velocities of 74763 km/s and 73044 km/s, respectively. The K-correction for E/SO galaxies is computed using the spectral energy distribution of an old elliptical galaxy and the filter response. The synthetic spectrum was obtained through the GISSEL96 evolutionary code (Bruzual & Charlot 1993), with the Miller & Scalo IMF (1979) and solar metallicity. In their analysis

of a statistical sample of 116 nearby Abell clusters, Hoessel et al. (1980) found an average value of $M_V = -22.68 \pm 0.03$ for the cluster BCG's with a dispersion of 0.35 magnitudes within a 16.4 kpc aperture. We have calculated the K-corrected absolute magnitude in this same aperture (4 arcsec at the redshift of Abell 521) and using the same cosmological parameters ($H_0 = 60$ km/s/Mpc), and we obtained respectively: $M_V = -22.57$, $M_V = -22.28$ and $M_V = -22.37$ for the BCG, galaxy 10, and galaxy 20, which are all within 1.5σ of their findings. Thus Abell 521 includes, besides the BCG, two other giant elliptical galaxies of central absolute magnitude typical of brighter cluster members. These objects could be interpreted, in the hierarchical scenario in which rich clusters form from the aggregation of smaller units, as the main galaxies of the groups which have collided. The presence of these giant ellipticals, which are expected to eventually accrete to the most massive giant elliptical, would then suggest that we are seeing the early stage of the formation of the cluster.

The BCG in Abell 521 extends over at least 20×30 arcsec, which corresponds to spatial dimensions of $90 \times 150 h_{50}^{-1}$ kpc. This is why, although the BCG luminosity obtained within the previous small apertures is comparable to the other two giant ellipticals, its asymptotic total luminosity is significantly larger. In fact, its high absolute luminosity and large dimensions are quite characteristic of a cD galaxy. However, the original definition of a cD galaxy (Matthews et al. 1964) also requires that it be embedded in an extended luminous envelope which is generally detected as a flattening of the slope in the surface brightness profile at large radius (see also Schombert 1988). Unfortunately, our image is neither deep enough nor large enough to detect the existence of such a halo. We are therefore unable, with the present data, to disentangle between the cD/D/gE classifications for the BCG. If the BCG is a cD galaxy, then in this analysis we are missing the contribution of the halo to the total luminosity, and our measured magnitude is probably under-estimated.

4.2. The core of the BCG

The very central region around the BCG galaxy shows a complex structure. In the inner region of $20 h_{50}^{-1}$ kpc, one can notice a bright secondary nucleus, A1, and three faint ones: A2, A3, and A4 (see Figure 8). Multiple nuclei in brightest cluster galaxies have shown to be quite a frequent phenomena. Various systematical studies of samples of BCGs in clusters (Tonry 1985; Hoessel and Schneider 1985) have shown that about 50% of BCGs have at least one extra nucleus within $20 h_{50}^{-1}$ kpc. Only a small fraction of these occurrences have been shown to be attributed to spurious projections. We successfully measured the redshift of nucleus A1 (73857 ± 55 km/s), confirming its status as a cluster member. Although we did not measure the redshift of the fainter nuclei A2, A3, and A4, their color

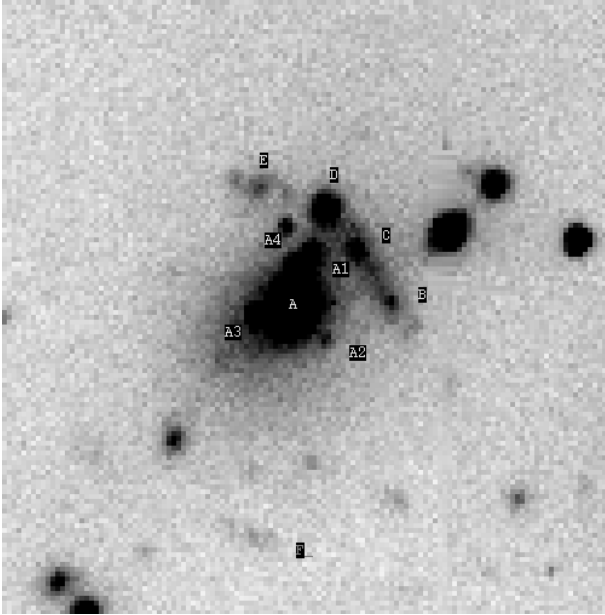


Fig. 8. Close-up on the region of the Brightest Cluster Galaxy. Multiple nuclei are apparent near the central galaxy A (e.g., A1, A2, A3, and A4). The giant arc candidate is visible to the northwest at a distance of ~ 7 arcsec from the BCG galaxy as a diffuse structure with brighter knots superimposed (B, C, D, and E). A smaller arc candidate (F) is visible at 14 arcsec to the South.

indexes are rather similar to those of A1, and are thus expected to be members of the cluster as well. The velocity measurement of nucleus A1 shows a significant peculiar motion with respect to the BCG of $-413 \pm 57 \text{ km/s}$ in the local rest frame. These results suggest that the region of the BCG is still experiencing strong dynamical activity, and that, according to the scenario of Hausman and Ostriker (1978), the multiple nuclei are the remnants of galaxies absorbed by the BCG by cannibalism.

4.3. The giant gravitational arc candidate revisited

Roughly 7 arcsecs to the Northwest of the BCG, one can see the giant arc candidate studied by Maurogordato et al. (1996) (Figure 8). It spreads over the northwest quadrant more than 10 arcsecs, with a radius of curvature of ~ 7.5 arcsecs, and it is nearly centered on the BCG. The structure is clumpy and appears as a chain of several bright condensations (B, C, D, and E) superimposed on a possible diffuse component. Also, an arclet candidate appears 14 arcsecs to the South (F). The mean magnitudes and colors for the central galaxy and the different knots found in this area are listed in Table 4. The colors of the brightest knot D are fully compatible with the expected value for an elliptical galaxy at the cluster velocity, and it is also in good agreement with the colors observed for the brightest galaxies in the cluster core. The velocity of this

object ($74379 \pm 72 \text{ km/s}$) clearly identifies it as a cluster member. A moderate signal-to-noise spectrum of knot D is presented in Figure 9, and compared to a synthetic spectrum of a E-type galaxy. The condensations along the arc candidate display different colors in the filter-bands available. This fact strongly argues against the hypothesis of a single multiple-image system.

We would like now to compare the spectral energy distribution of the three knots in detail. On this purpose, as no spectrophotometric standard star was observed during our run, we have used the good-quality spectrum of knot D to flux calibrate the other two components (Figure 9). As knot D exhibits all the spectral features expected for a typical elliptical galaxy, a synthetic E-type continuum was used for this exercise, taken from the GISSEL evolutionary code (Bruzual and Charlot 1993, updated in 1998). Knots C and D have the same redshift within the errors ($z = 0.248$). The spectrum of knot B is noisier, but its redshift is also compatible with that of the cluster ($z = 0.25$, see Table 4). The spectra of these knots become bluer from D to B, as expected from their $B - R$ colors. At the redshift of this cluster, the $B - R$ color index is a good measure of the Balmer break, or the 4000 \AA break. Furthermore, the relative strength of the redder Balmer absorption lines increases from D to B. Knot C exhibits absorption lines similar to those found in spiral galaxies at such a resolution, whereas knot B displays much stronger Balmer lines. Unfortunately, the poor quality of the knot B spectrum precludes a careful synthesis of the stellar population. Although a more careful analysis of these objects is needed, based on spectra with better signal-to-noise ratios, these preliminary results indicate a clear change in the properties of the stellar population along the arc. If one interprets the change in Balmer line strengths as indicative of an age sequence, knot B is the younger, and the mean age of the underlying stellar population increases towards knot D.

According to these results, the three brightest knots of the arc structure seen in Abell 521 are in fact cluster galaxies. This result does not completely exclude the gravitational lensing hypothesis for the other arclet candidates in this region (E,F). A deep photometric multi-color survey is required for further progress, in particular to identify possible background sources using photometric redshift techniques.

4.4. Peculiar motion of the BCG ?

In most theories of BCG formation in clusters, these objects are required to occupy the bottom of the cluster gravitational potential. However, there have been suggestions of evidence for at least some BCGs presenting significant velocity offsets as compared to the velocity location of the cluster as a whole (Oegerle and Hill 1994). It has been pointed out that many of the apparently large peculiar velocities seem to be correlated with the presence of sub-

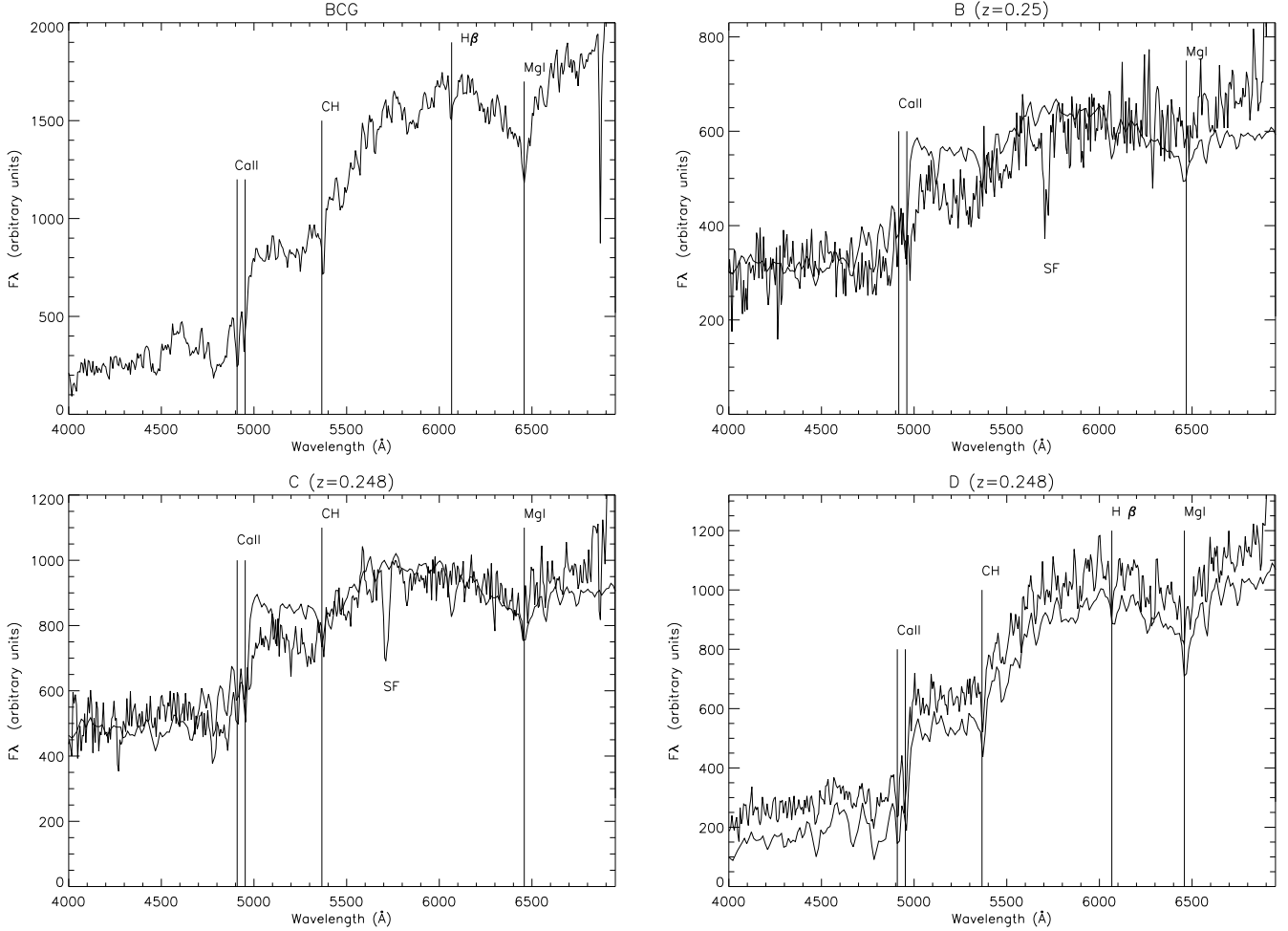


Fig. 9. Spectra of the BCG (Top-left), and of the various bright components of the arc: knot B (Top-right), knot C (Bottom-left), Knot D (Bottom-right). A synthetic spectrum of an S-type galaxy is superimposed on the spectrum of B and C for comparison. An E-type synthetic spectrum is overplotted on the spectrum of the bright knot D.

structure, and have been claimed to represent a signature of recent (or ongoing) subcluster merger events (Bird 1994). Moreover, at the bottom of the cluster potential the effect of the gravitational redshift becomes non-negligible (Nottale 1983); as shown by Cappi (1995), in rich clusters this effect gives a significant positive velocity difference between the BCG and the cluster and, while in principle detectable only statistically with a large number of clusters, it represents an additional source of uncertainty for the estimate of the BCG peculiar velocity.

Care must be taken when evaluating the significance of a proposed BCG velocity offset (see the discussion in Gebhardt and Beers 1991), taking appropriate estimates of errors in central location on velocity into account. As we are confronted with observational evidence of merging activity in Abell 521, we are particularly interested in quantifying whether a peculiar offset of the BCG does in fact exist. The BCG galaxy of Abell 521 has a velocity $v_{BCG} = 74374 \pm 47 \text{ km/s}$, slightly higher than the central velocity location of the cluster as a whole

$C_{BI} = 74132^{+202}_{-250} \text{ km/s}$. This results in a peculiar velocity $v_{pec} = +242 \text{ km/s}$, which has to be corrected by $(1+z)$ to obtain the peculiar motion in the cluster rest frame: $v_{pec} = +194 \text{ km/s}$. Since we have argued above that the kinematics of Abell 521 may in fact be rather complex, we have also calculated the velocity offset of the BCG with respect to the *red* subset of velocities. After correction to the cluster rest frame, we obtain a similar peculiar velocity: $v_{pec} = +200 \text{ km/s}$.

Are either of the above offsets statistically significant? Gebhardt and Beers (1991) outline a prescription for answering this question, based on a comparison of the measured (rest frame) velocity of the BCG with respect to the biweight estimator of velocity central location for the parent cluster or subcluster, with bootstrapped (90%) confidence intervals on the velocity central location. The 90% confidence interval on velocity location for the entire set of galaxies is $[-398, +327] \text{ km/s}$; that for the *red* subsample is $[-432, +371]$. The 90% measurement error for the BCG velocity is $\pm 78 \text{ km/s}$. Thus, in both instances, the

peculiar velocity of the BCG is completely contained within the 90% interval on central location in velocity space, and neither offset can be considered significant. This probe could be substantially improved by obtaining a larger set of galaxies with measured velocities in Abell 521, in order to shrink the confidence intervals on location in velocity space.

We have also calculated the peculiar velocities of the two bright elliptical galaxies (10 and 20) and obtain rest-frame peculiar velocities of $v_{pec} = +506 \text{ km/s}$ and $v_{pec} = -872 \text{ km/s}$, respectively, when compared to the cluster as a whole. When compared to the *red* subsample, the peculiar velocities are $v_{pec} = +512 \text{ km/s}$ and $v_{pec} = -867 \text{ km/s}$, respectively, which are essentially the same. The 90% measurement errors for the observed velocities of these galaxies are ± 88 and $\pm 150 \text{ km/s}$, respectively. The velocity offset of galaxy 10 is thus judged to be statistically significant, when compared to either the entire cluster or the *red* subsample. The 90% confidence interval on the measured velocity fails to overlap with the 90% confidence intervals on the central locations in either instance. An even greater significance is attached to the velocity offset of galaxy 20.

5. Discussion and Conclusions

From the analysis of our data obtained through multi-object spectroscopy, we have found that Abell 521 is a moderately distant cluster ($z = 0.2467$) with an apparently very large velocity dispersion ($S_{BI} = 1386 \text{ km/s}$). The velocity distribution of cluster members is consistent with sampling from a parent Gaussian population, and the high dispersion does not seem to result from trivial superposition effects. However, there do exist several hints that this large apparent velocity dispersion may be due to a superposition of several distinct populations of galaxies. The projected distribution of the galaxy positions in the cluster can be described with a mixture of three two-dimensional Gaussians, a model which is significant at the 99% level. Analysis of the velocity distribution for these partitions shows that the velocity dispersion is very high ($\sim 2000 \text{ km/s}$) in the central North-East/ South-West “ridge” corresponding to KMM2 North, although the dispersion for the smaller samples of galaxies associated with the KMM1 and KMM2 South partitions are more typical of most rich clusters ($\sim 800 \text{ km/s}$). We also find that the velocity distribution is rather different for subsets of the galaxies selected according to color, with the bluest objects (spirals) showing a high velocity dispersion ($\sim 1800 \text{ km/s}$) and the redder objects (ellipticals) exhibiting a much smaller dispersion ($\sim 1000 \text{ km/s}$). This is another indication that this cluster is dynamically young, with its population of spirals not yet relaxed to the cluster potential. Moreover, the high value of the velocity dispersion as compared to the one expected from the X-Ray Temperature from the σ/T relation suggests that this cluster is far from dynamical equilibrium.

On the basis of our results, we can outline a tentative picture of the dynamical state of Abell 521. In the frame of hierarchical models, the cluster formation process proceeds by merging of smaller units (Frenk et al. 1996). Several evidences that merging processes are occurring in this cluster have been suggested in the previous analysis.

However, one can note that the various clumps evidenced on the NW/SE axis (KMM1, KMM2 South, KMM3) are well-defined concentrations. The foreground/background hypothesis is quite improbable, as redshift measurements have shown that all the groups contain several cluster members (although in the case of KMM3 only two redshift measurements exist). We are then probably seeing the early phase of infall of these various groups. According to numerical simulations (Schindler and Bohringer 1993), we should expect that groups are strongly accelerated and their velocity distributions diverge as the merger process proceeds. However, we do not detect any offset of the central velocity locations of the various groups (except possibly KMM3, which could be at a slightly higher velocity of $\sim 75800 \text{ km/s}$ based on the two measured velocities). This implies that either we are seeing the very beginning of the merging and the clumps are still close to at rest with respect to one another, or we are witnessing a more advanced state but fail to detect the shift of the velocity distributions because the collision axis happens to be mostly in the plane of the sky.

The apparently large velocity dispersion of Abell 521 is due in great part to the contribution of the KMM2 North structure. Its very high velocity dispersion suggests that we are witnessing the collision epoch, at which point numerical simulations show that the dispersion reaches its maximum value, which can be twice the value after the cluster approaches dynamical equilibrium (Schindler and Bohringer 1993). The present data could be explained in a scenario whereby two (or more) subclusters have just collided along an axis which is projected on the sky in the direction of KMM2 North, but with a substantial component along the line of sight. The large peculiar velocities of the two bright elliptical galaxies of the cluster is an indication that they probably originated in different initial subclusters, as has been seen in other clusters (e.g., Abell 2255, Burns et al. 1995). A detailed merging scenario taking into account the whole set of optical and X-Ray properties of this cluster is presented in Arnaud et al. 1999.

The region surrounding the Brightest Cluster Galaxy is particularly interesting. The inner part of the BCG ($20h_{50}^{-1} \text{ kpc}$) exhibits multiple nuclei, one of which (A1) exhibits a significant velocity offset with respect to the main body of the BCG (A). These facts suggest the possibility of strong merging activity. At larger distance from the BCG ($30h_{50}^{-1} \text{ kpc}$) a curved structure is seen, with three knots superimposed. Analysis of the spectra and colors of the knots suggest that at least two of them are in fact galaxies belonging to the cluster. The spectrum of the

third knot has a low signal-to-noise ratio, but seems to also be at a redshift typical of the cluster. This calls into question the gravitational lensing hypothesis to explain the arc-like structure, and favors the interpretation as an effect of merging. The colors of the two arclet candidates E and F suggests these should be high-redshift objects. Deep multiband observations are necessary to constrain the redshift range of the knots by the technique of photometric redshifts. Additional multi-object spectroscopy in order to obtain a complete set of velocity information for galaxies in Abell 521 down to magnitude $m_V = 21$ would be crucial for our understanding of the dynamical state of this apparently highly unrelaxed cluster.

Acknowledgements. We would like to thank C. Vanderriest and O. Le Fèvre for the acquisition of the first images of Abell 521 at CFHT, with Alain Mazure for fruitful discussions on the dynamics of this cluster.

References

- Abell, G.O., 1958, *ApJS*, 3, 211
- Abell, G.O., Corwin, H.G., Olowin, R.P. 1989, *ApJS*, 70, 1
- Arnaud, M., Maurogordato, S., Slezak, E., Rho, J., 1999, in preparation
- Beers T., Flynn K., Gebhart K., 1990, *AJ* 100, 32
- Beers T., Flynn K., Gebhart K., Huchra, J., Forman, W., Jones, C and Bothun, G., 1992, *ApJ*, 400, 410
- Binggeli B., Tammann G.A., Sandage A., 1987, *AJ* 94, 251
- Bird, C.M., 1994, *AJ* 107, 1637
- Bird, C.M. and Beers, T., 1993, *AJ*, 107, 1637
- Bird, C.M., Davis, D., and Beers, T., 1995, *AJ*, 109, 920
- Bruzual, A., G., Charlot, S., 1993, *ApJ*, 405, 538
- Burns, J., Roettiger, K., Pinkney, J., Perley, R., Owen, F., and Voges, W., 1995, *ApJ*, 446, 583
- Cappi A., 1995, *A&A* 301, 6
- Fort, B. and Mellier, Y., 1994, *A&ARv*, 5, 239
- Frenk, C., Evrard, A., White, S., Summers, F., 1996, 472, 460
- Gebhardt, K. and Beers, T.C., 1991, *ApJ*, 383, 72
- Girardi, M., Fadda, D., Giuricin, G., Mardirossian, F., Mezzetti, M., Biviano, A., 1996, *ApJ*, 457, 61
- Henry, J.P., Briel, U.G., Nulsen, P.E.J., 1993, *A&A* 271, 413
- Hoessel, J.G., Gunn, J.E., and Thuan, T.X., 1980, *ApJ*, 241, 486
- Hoessel, J.G. and Schneider, D.P., 1985, *AJ*, 90, 1648
- Hausman, M.A., and Ostriker, J.P., 1978, *ApJ*, 224, 320
- Jones, B. J. T., & Mazure, A. 1996, in Mapping Measuring, and Modell ing the Universe, ASP Conference Series, 94, eds. P. Coles, V. J. Martinez & M.-J. Pons-Borderia (San Francisco: Astronomical Society of the Pacific), p. 197
- Kowalski, M.P., Ulmer, M.P., Cruddace, R.G., Wood, K.S., 1984, *ApJS* 56, 403
- Kriessler, J.R. and Beers, T.C., 1997, *AJ*, 113, 80
- Le Fèvre O., Crampton C., Felenbok, P., and Monnet, G., 1994, *A&A*, 282, 325
- Le Fèvre O., Crampton C., Lilly S.J., Hammer F., Tresse L., 1995, *ApJ*, 455, 60
- Matthews, T.A., Morgan, W.W., and Schmidt, M., 1964, *ApJ*, 140, 35
- Mazure, A., Katgert, P., den Hartog, R., Biviano, A., Dubath, P., Escalera, E., Focardi, P., Gerbal, D., Giuricin, G., Jones, B., Le Fèvre, O., Mole s, M., Perea, J., Rhee, G., et al., 1996, *A&A*, 310, 31
- Maurogordato S., Le Fevre, O., Proust, D., Vanderriest, C., Cappi, A., 1996, *BCFHT*, 34, 5
- Merritt, D. and Gebhardt, K., 1995, XXIXe Moriond Astrophysics Meetings F. Durret, A. Mazure, J. Tran Thanh Van eds, Editions Frontieres, p 11.
- Miller G.E., Scalo J.M., 1979, *ApJS* 41, 513
- Nottale L., 1983, *A&A* 118, 85
- Oegerle, W., and Hill, J., 1994, *AJ*, 107, 857
- Pelló et al., 1999, in preparation
- Schindler, S., and Bohringer, H., 1993, *A&A*, 269, 83
- Schombert, 1988, *ApJ*, 328, 475
- Slezak et al., 1999, in preparation
- Tonry J., Davis, M., 1981, *ApJ* 84, 1511
- Tonry, J., 1985, *AJ*, 90, 2431
- Tully, R.B., Shaya, E.J., 1984, *ApJ*, 281, 31.
- Zabludoff, A., Huchra, J., Geller, M.J., 1990, *ApJS*, 71, 1

Table 1. Heliocentric redshifts in the 10'x10' frame centered on Abell 521.

| NUMBER | R.A. (2000) | DEC. (2000) | HEL. VEL. v (km s ⁻¹) | ERROR Δ v (km s ⁻¹) | emission lines |
|--------|----------------|----------------|---------------------------------------|--|-------------------------|
| 1 | 4:54:20.5 | -10:12:30.8 | 74298 | 84 | |
| 2 | 4:54:18.4 | -10:14:15.9 | 28324 | 24 | |
| 3 | 4:54:15.1 | -10:15:52.5 | 72534 | 78 | |
| 4 | 4:54:13.8 | -10:13:34.2 | 88586 | 102 | |
| 5 | 4:54:12.7 | -10:15:52.3 | 73805 | 38 | |
| 6 | 4:54:12.3 | -10:13:48.4 | 76607 | 57 | |
| 7 | 4:54:11.5 | -10:14:20.5 | 72071 | 54 | |
| 8 | 4:54:10.7 | -10:14:28.9 | 73885 | 73 | |
| 9 | 4:54:09.3 | -10:14:48.4 | 76630 | 48 | |
| 10 | 4:54:08.6 | -10:14:24.3 | 74763 | 53 | |
| 11 | 4:54:08.1 | -10:12:53.8 | 74873 | 67 | |
| 12 | 4:54:05.7 | -10:13:01.4 | 73640 | 64 | |
| 13 | 4:54:04.2 | -10:13:17.3 | 86725 | 206 | |
| 14 | 4:54:03.5 | -10:13:02.9 | 75146 | 59 | |
| 15 | 4:54:02.2 | -10:12:51.8 | 99306 | 33 | [OII],H β ,[OIII] |
| 16 | 4:54:01.1 | -10:13:07.9 | 73837 | 89 | |
| 17 | 4:53:59.7 | -10:12:19.9 | 70699 | 72 | |
| 18 | 4:53:58.7 | -10:15:13.0 | 74604 | 63 | |
| 19 | 4:53:57.9 | -10:12:11.1 | 74846 | 93 | |
| 20 | 4:53:57.0 | -10:12:44.9 | 73044 | 90 | |
| 21 | 4:53:55.3 | -10:14:17.9 | 75759 | 56 | [OII] |
| 22 | 4:54:06.2 | -10:15:53.1 | 73317 | 81 | |
| 23 | 4:54:07.0 | -10:14:44.8 | 71584 | 79 | |
| 24 | 4:54:07.9 | -10:15:36.4 | 77596 | 38 | |
| 25 | 4:54:08.8 | -10:14:33.9 | 74727 | 40 | |
| 26 | 4:54:09.7 | -10:16:19.8 | 75692 | 94 | |
| 27 | 4:54:10.5 | -10:14:52.6 | 70522 | 112 | [OII] |
| 28 | 4:54:13.1 | -10:15:09.7 | 75002 | 88 | |
| 29 | 4:54:14.1 | -10:15:50.1 | 73381 | 57 | |
| 30 | 4:54:14.7 | -10:15:37.7 | 74874 | 36 | |
| 31 | 4:54:06.2 | -10:13:19.8 | 74435 | 42 | |
| 32 | 4:54:06.8 | -10:13:59.4 | 73025 | 51 | |
| 33 | 4:54:07.7 | -10:13:44.9 | 72150 | 61 | |
| 34 | 4:54:05.9 | -10:13:00.2 | 73704 | 93 | |
| 35 | 4:54:09.3 | -10:14:10.7 | 76736 | 76 | |
| 36 | 4:54:07.2 | -10:16:54.3 | 73219 | 60 | |
| 37 | 4:54:08.1 | -10:16:10.0 | 70225 | 97 | [OII] |
| 38 | 4:54:15.4 | -10:16:52.5 | 109645 | 74 | |
| 39 | 4:54:16.5 | -10:16:37.0 | 92925 | 150 | [OII] |
| 40 | 4:54:18.5 | -10:16:51.4 | 88450 | 85 | [OII] |
| 41 | 4:54:19.0 | -10:17:39.4 | 75852 | 52 | |
| 42 | 4:54:15.4 | -10:16:14.4 | 74055 | 80 | |
| 43 | 4:54:17.4 | -10:18:08.0 | 75799 | 62 | |
| 44 | 4:54:19.1 | -10:16:47.3 | 74073 | 74 | |
| 45 | 4:54:15.8 | -10:14:07.2 | 72967 | 84 | |
| 46 | 4:54:19.9 | -10:13:22.7 | 88820 | 41 | [OII] |
| 47 | 4:54:23.4 | -10:12:24.7 | 75428 | 86 | |
| 48 | 4:54:24.3 | -10:12:01.1 | 72048 | 82 | |
| 49 | 4:54:06.9 | -10:13:24.7 | 74374 | 47 | |

Table 2. Mixture Model Parameters for Abell 521

| group | N_g | % N_{tot} | % L_{tot} | $x \pm \sigma_x$ (arcmin) | $y \pm \sigma_y$ (arcmin) | m_{med} (V) | m_{10-20} (V) |
|-------|-------|-------------|-------------|------------------------------|------------------------------|------------------|--------------------|
| (1) | (2) | (3) | (4) | (5) | (6) | (7) | (8) |
| 1 | 184 | 46 | 46 | 1.8 ± 1.7 | 0.9 ± 2.4 | 21.0 | 19.3 |
| 2 | 160 | 40 | 47 | -1.6 ± 1.4 | 0.0 ± 2.3 | 20.9 | 19.4 |
| 3 | 52 | 13 | 7 | -2.4 ± 1.0 | -3.4 ± 0.7 | 21.2 | 20.7 |

Table 3. ROSTAT analysis of velocity samples in Abell 521

| sample | N_v | v_{BI} | S_{BI} | AI | TI |
|-------------|-------|-----------------------|----------------------|-------|------|
| All | 41 | 74132^{+202}_{-249} | 1386^{+206}_{-139} | -0.24 | 1.17 |
| KMM1 | 9 | 74124^{+289}_{-232} | 806^{+682}_{-240} | -0.65 | 1.74 |
| KMM2 (N) | 14 | 74122^{+552}_{-650} | 1994^{+328}_{-226} | -0.37 | 0.75 |
| KMM2 (S) | 5 | 73751^{+228}_{-390} | 747^{+276}_{-57} | -0.11 | |
| <i>red</i> | 19 | 74125^{+218}_{-273} | 1011^{+214}_{-108} | +0.49 | 1.19 |
| <i>blue</i> | 20 | 73924^{+408}_{-445} | 1803^{+256}_{-191} | -0.09 | 0.96 |

Table 4. Characteristics of the knots around the BCG in Abell 521

| knots | R | B | V | J | $B - R$ | $B - V$ | $V - J$ | v (km/s) | Δv (km s ⁻¹) |
|-------|-------|-------|-------|-------|---------|---------|---------|------------|-----------------------------------|
| A | 17.42 | 20.41 | 18.58 | 15.54 | 2.99 | 1.83 | 3.04 | 74374 | 47 |
| A1 | 19.27 | 22.24 | 20.40 | 16.88 | 2.97 | 1.84 | 3.52 | 73857 | 55 |
| B | 20.54 | 22.65 | 21.54 | 18.56 | 2.11 | 1.11 | 2.98 | 75600 | 600 |
| C | 20.17 | 22.47 | 21.11 | 17.99 | 2.30 | 1.36 | 3.12 | 74370 | 300 |
| D | 19.79 | 22.50 | 20.92 | 17.88 | 2.71 | 1.58 | 3.04 | 74370 | 72 |
| E | 21.12 | 22.85 | 21.91 | 18.95 | 1.73 | 0.94 | 2.96 | | |
| F | 22.35 | 23.69 | 23.00 | 21.17 | 1.34 | 0.69 | 1.83 | | |